# Chapter 6
# Aerogel Nanomaterials for Dye Degradation


**Sanjana Jacob, S. Kaviya, and K. Anand**

**Abstract** Water pollution has been considered as a major environmental issue that has become a threat to human health. Therefore, an efficient solution for removing pollutants from water is needed. One such efficient solution for the removal of pollutants is by using aerogels. Due to their high absorption rate and properties, aerogels exhibit a wide range of properties and hence can be chosen for demanding applications. It has been proven that the characteristic features like exceptionally high porosity, huge specific surface area, very low density, ease of detachment from aqueous solution etc. make these materials suitable for dye removal. The current chapter deals with the study of aerogel materials, classification, synthesis (some selected aerogel materials) and their dye degradation and photocatalytic applications.

**Keywords** Aerogel · Nanomaterials · Synthesis · Dye degradation · Photocatalysis

## 6.1 Introduction

Water pollution has been considered as a major environmental issue, that has become a threat to human health. Organic pollutants and its toxic substances in the waste water not only destroy the ecosystem, but also significantly affect the aquatic life. Therefore, an efficient solution for the removal of pollutants from water is needed.

S. Jacob
Department of Nanotechnology Engineering, Srinivas Institute of Technology, Mangalore, Karnataka 574143, India

S. Kaviya
Department of Chemical Engineering, Birla Institute of Technology and Science, BITS Pilani Hyderabad Campus, Hyderabad, Telangana 500078, India

K. Anand (✉)
Department of Basic Sciences, Amal Jyothi College of Engineering, Kanjirapally, Kerala 686518, India
e-mail: anand.rrii@gmail.com

Apcotex Industries Limited, Plot No.3/1, MIDC Industrial Area, Taloja, Dist. Raigad, Maharashtra 410208, India

© The Author(s), under exclusive license to Springer Nature Switzerland AG 2022

S. Dave and J. Das (eds.), *Trends and Contemporary Technologies for Photocatalytic Degradation of Dyes*, Environmental Science and Engineering,
https://doi.org/10.1007/978-3-031-08991-6_6

Various technologies are proposed to erase such pollutants in the water like oxidation, adsorption, photocatalysis degradation, electron degradation etc. (Wu et al. 2020). Aerogel materials due to their large surface area and absorption capacity can play a major role in dye degradation. In this chapter the usage of aerogel nanomaterials for dye degradation particularly, the photocatalytic degradation properties of different aerogel materials are discussed.

### *6.1.1 Aerogel—Overview*

Aerogel materials have three-dimensional open network that are arranged by the structured nanoparticles/polymer molecules (Fricke 1988; Fricke and Emmerling 1998; Pierre and Pajonk 2002; Vacher et al. 1988). The aerogel was first made by Kistler in 1931. It was called "aerogel" which is air and gel because it replaced liquid element inside of the wet gel with the air not destructing solid micro structure (Du et al. 2013). Aerogels are the sol–gel traced solid material that has porousness about 80–99.8%. The advanced level porosity was gained through the supercritical drying of the alcogel or the hydrogel in autoclave (Fricke et al. 1992). In the recent developments, it states that aerogel could also be recognized as a new state of matter (Wagh et al. 1999) and also aerogel shows qualitative variation in the bulk property when compared with the other states of matter. Aerogel maintains a fixed shape and volume like that of the solids and the density of the aerogel may extend between 1000 and 1 kg/m$^3$. Aerogel exhibits unique properties like low density solid, reduced thermal conductivity, low sonic velocity, low refractive index, reduced dielectric constant, reduced sound speed and broad specific surface area (Fricke and Emmerling 1998; Pierre and Pajonk 2002; Schaefer and Keefer 1986; Gesser and Goswami 1989). The structure of aerogel can be defined using the electron microscope, pore size analyzer, small angle X-ray scattering etc. Properties are measured by particular instruments, for example, mechanical properties of aerogel can be tried/tested by the accurate UTM or the dynamic thermo-mechanical analyzer in compression or the three-point bend type. All kinds of ultra-light foams cannot be categorized as aerogel state (Du et al. 2013; Schaedler et al. 2011).

## 6.2 Classification, Properties and Applications

Aerogels can be classified using different methods: based on the appearance, they are classified into monolith, film and powder. Based on the preparation techniques, they are classified into aerogels, xerogels and cryogels. Classifications of aerogels are shown in Fig. 6.1 (Nita et al. 2020). From this figure, one understands that aerogels can be separated into two categories: inorganic and organic. Inorganic aerogels is further subdivided into five categories: Fluoride, Silica, Metal, Oxides and Chalcogens. Organic is subdivided into two: Polymer and Carbon based (Du et al. 2013).

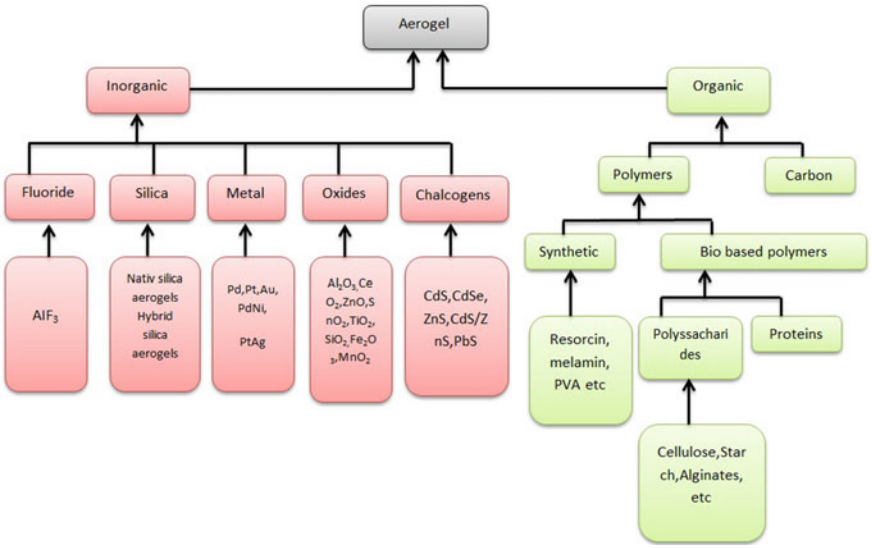


**Fig. 6.1** Classification of aerogels (Nita et al. 2020). (Reproduced from reference (Nita et al. 2020) open access)

The unique properties of aerogel make them attractive in technology and science. Based on their properties, aerogels can be used for different applications (Table 6.1).

## *6.2.1 Synthesis of Aerogel Materials*

### Sol–gel method of synthesis

Sol–gel action of synthesis is the most popular and trusted way for the synthesis of the materials, specifically the metal oxides that have regular small particle size and with different morphologies. It consists of the transformation of the system from the liquid sol into the solid gel phase (Gurav et al. 2010).

The sol–gel way for the synthesis/preparation of aerogel can normally be separated into the following steps: as in Fig. 6.2 (Du et al. 2013).

(a) Solution—sol formation: Nanoscale sol substances are created in the precursor solution spontaneously or that are catalyzed by the catalysts through condensation and by hydrolysis reactions.
(b) Sol-gel formation (Gelation): The substances that are the sol are cross linked and arranged into a wet gel with coherent network hierarchically.
(c) Gel-aerogel formation (Drying and Densification): Solvent in the wet gel is replaced by the air without damaging the microstructure seriously, and then it is densified (Du et al. 2013).

**Table 6.1** Application of aerogel with respect to properties adapted with permissions from (Gurav et al. 2010)

| Property | Feature | Application |
|---|---|---|
| Mechanical | i. Its elastic<br>ii. Its light weight | i. Hypervelocity particle trap<br>ii. Energy absorber |
| Electrical | i. The lowest dielectric constant<br>ii. The high dielectric strength<br>iii. The high surface area | i. In dielectrics for ICs<br>ii. In spacers for vacuum electrodes<br>iii. In capacitors |
| Acoustic | i. The low speed of sound | i. In sound proof rooms<br>ii. In acoustic impedance matching in ultrasonic distance sensors |
| Optical | i. Transparent<br>ii. The low refractive index<br>iii. The multiple composition | i. Light weight optics<br>ii. Cherenkov detectors<br>iii. Light guides |
| Density/porosity | i. Lightest synthetic solid<br>ii. High surface area<br>iii. Multiple compositions | i. For catalysis<br>ii. In sensor<br>iii. For fuel storage<br>iv. In ion exchange<br>v. For filters for pollutants gaseous<br>vi. In targets for ICF<br>vii. In pigment carriers<br>viii. As template |
| Thermal conductivity | i. The best insulating solid<br>ii. Transparent<br>iii. It withstands high temperature<br>iv. Its light weight | i. In building construction and appliance insulation<br>ii. In storage media<br>iii. In automobiles, space vehicles<br>iv. In solar devices, solar ponds |

The main advantage of sol–gel process is its simplicity and are economical. It is one of the effective ways of producing materials that are of high quality. The processing of sol–gel technique finds application in high-quality glass production for fibers and optical components, fine powders of oxides and thin-film coatings (Gurav et al. 2010; Matsuda et al. 2000; Torikai et al. 1994; Hamaker 1937).

Though different types of aerogel materials are available, herein, we discuss the synthesis of some selected aerogel nanomaterials as given below:

a. $TiO_2$@CNF aerogel
b. $SiO_2$ aerogel
c. 3D nitrogen-doped graphene aerogel
d. Synthesis of $MoS_2$ aerogel
e. PTA/ZIF-8@cellulose aerogel.

### $TiO_2$@CNF aerogel synthesis

$TiO_2$@CNF aerogel is created by the combination of sol–gel method and hydrothermal method. CNF aerogels were soaked for about 30 min in the mixed solution of $Ti(OC_4H_9)_4$ and absolute ethanol, and then the aerogel was taken out. The remaining $Ti(OC_4H_9)_4$, which was not absorbed, were washed out by absolute

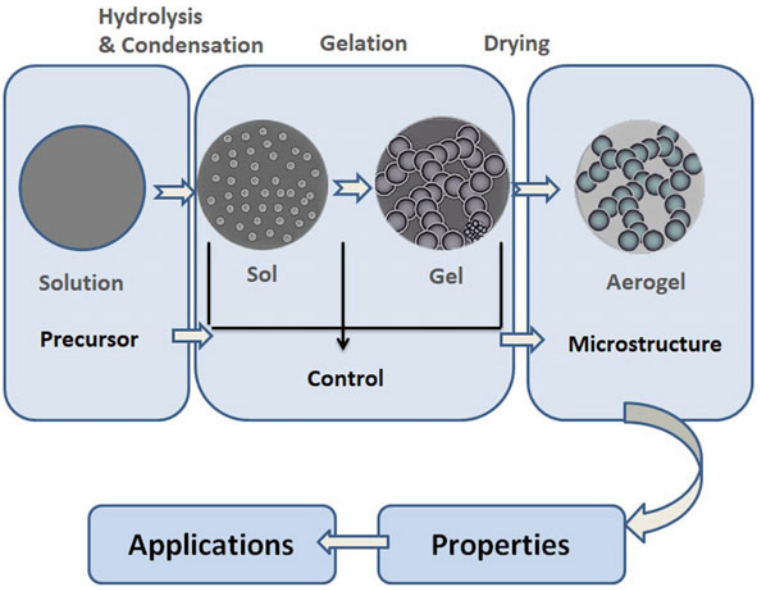


**Fig. 6.2** The schematic demonstration showing the synthesis of the aerogel materials by sol–gel process (Du et al. 2013). Reproduced with permissions from reference (Du et al. 2013)

ethanol. Later the gel is immersed in a blended sol of water and absolute ethanol in a ratio of volume 4:1, and the pH adjusted to 3.0 with the dilute HCl. The gel is left undisturbed for 2 h to confirm that $Ti(OC_4H_9)_4$ gets hydrolyzed completely. The intermediate is placed onto a PTFE-lined hydrothermal reactor that is reacted at 120 °C for the variable duration to understand the optimum time of reaction. The freeze-drying process takes place to get $TiO_2$@CNF aerogel. The processes like absorption, hydrothermal and hydrolysis are repeated 1–5 times to get the aerogel loaded with different quantity of $TiO_2$ NPs (Li et al. 2021).

**$SiO_2$ aerogel**

For $SiO_2$ aerogel synthesis, 30 g of the rice husk ash is integrated along with 200 ml of 1 mol $L^{-1}$ sodium hydroxide (NaOH) solution. The aqueous solution is heated to 100 °C and then is left for 3.5 h. The pH (= 5) is altered by hydrochloric acid and ammonia solution. The removal of the Na ion from the sodium silicate through the cation exchange resin is done thereafter. After 24 h, hydrophobically modified silica aerogel is obtained by replacing the solvent with absolute ethanol, n-hexane and chlorotrimethylsilane (Liu et al. 2021).

**3D nitrogen-doped graphene aerogel (3DNG)**

g-$C_3N_4$ is dispersed into the 6.21 ml of distilled water through ultrasonication for about 6 h. The solution is then added into 3.72 ml of GO earlier for further ultra-sonication for the next 2 h. After that, 37.2 mg of urea and ascorbic acid of 9.3 mg

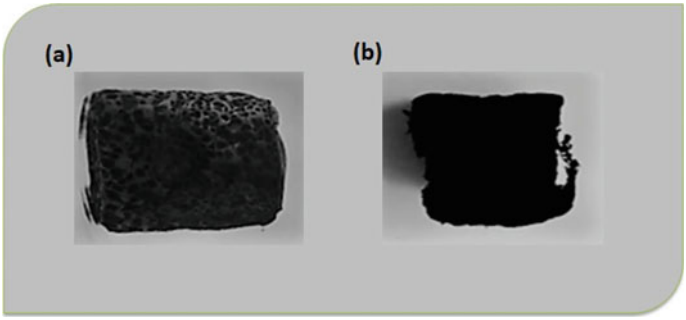


**Fig. 6.3** Picture of (**a**) three dimensional aerogel, (**b**) 3DNG. Adapted from (Maouche et al. 2020). Reproduced with permissions from reference (Maouche et al. 2020)

were then added and distributed into the solution for 1 h. The solution is covered and contained at 180 °C for about 6 h in the Teflon-lined autoclave, and it is made to cool naturally. As the method continues GO merges with g-$C_3N_4$ forming a three-dimensional porous reduced the GO. 3D graphene-supported aerogel is obtained as shown in Fig. 6.3(a) (Maouche et al. 2020).

Three-dimensional aerogel is formed after freeze-drying the three-dimensional hydrogel. It is heated for about 1 h under the Ar atmosphere at around 1000 °C and the 3D nitrogen-doped graphene aerogel that are thermally treated is obtained as in Fig. 6.3(b) (Maouche et al. 2020).

**Synthesis of $MoS_2$ aerogel**

For the synthesis of $MoS_2$ aerogel, 50 ml of the exfoliated $MoS_2$ solution is mixed with 5 mL of the 20% nafion solution and it is kept for sonication so that it can mix together and can form a uniform gel-like form of suspension. The container is then transferred to a 20 °C refrigerator for freezing the mixture. Later the solution that is frozen is freeze-dried in a lyophilizer at 60 °C and at $10^{-3}$ torr chamber to make $MoS_2$ aerogel (Peng et al. 2021).

**PTA/ZIF-8@cellulose aerogel**

The PTA/ZIF-8@cellulose aerogel composite material has a multi-layer 3D network shape. It is made using a cellulose aerogel framework. MOFs are used as filler and the preparation method is shown in Fig. 6.4. Steps involve freeze-drying, composition and impregnation (Wen et al. 2020).

#### 6.2.1.1 Different Dyes Used in Industries

Dyes have been used by various industries like textile, food, paper, cosmetic, leather, and fur with textile industry as a major consumer (Benkhaya et al. 2017). Apart from these, the dyes are used as indicators, hair coloring agents and in photography. The

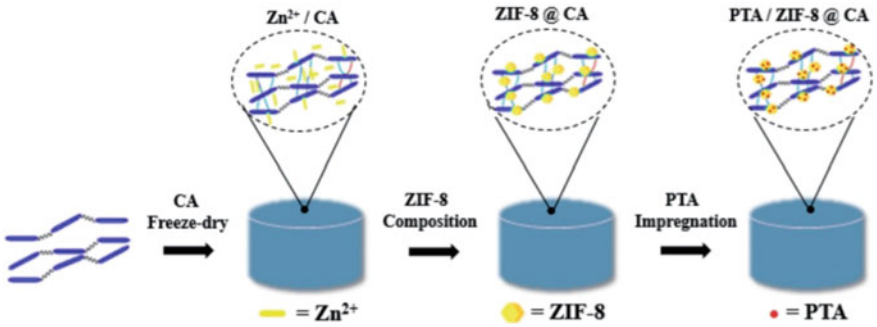


**Fig. 6.4** Preparation process of PTA/ZIF-8@cellulose aerogel. Adapted from (Wen et al. 2020). Reproduced with permissions from reference (Wen et al. 2020)

dyes were categorized based on their chemical structure, usage and application. Table 6.2 shows categorization of dyes based on usage or applications (Hunger 2007).

### *6.2.2 Dye Degradation using Aerogel Materials*

Degradation of dye involves the chemical breakdown of large dye molecules into smaller molecules. Removal of dye from industrial effluent is broadly classified into physical, chemical and biological methods, which are discussed in Table 6.3 (Siddiqui 2018). Aerogel materials are considered as one of the promising solutions for dye removal and can be synthesized in different forms using various methods. They are basically classified into inorganic aerogels, organic aerogels, and organic-inorganic hybrid aerogels materials (Hasanpour and Hatami 2020).

The inorganic aerogels are synthesized from almost all the metals or oxide semiconductors. These inorganic aerogels are traditionally prepared through hydrolysis and condensation methods. Semiconductor photocatalyst based aerogels such as $TiO_2$, $SiO_2$, ZnO and $InVO_4$ is analyzed for degradation of various pollutants. Among these, silica and titania were of greater interest because of its non-toxicity, less cost and photo-stability.

Xu et al. 2016a synthesized a binary aerogel of silicon dioxide/titanium dioxide by using sodium silicate and titanium tetrachloride as precursors. The surface modification of the material was performed to achieve the desired binary aerogel. The prepared aerogel shows notable photocatalytic activity for the degradation of methyl orange. It has achieved a photocatalytic efficiency of about 84.9% after exposure of the aerogel for 210 min under the irradiation of ultraviolet light. The degraded aerogel is reused and it shows 70% efficiency even after recycling the aerogel for about 4 times.

Zhang et al. (2018) prepared $TiO_2$ aerogel using a preceramic polymer as a precursor and bacterial cellulose as a bio template. The composite aerogel was

**Table 6.2** Categorization of the dyes based on its use or application. Adapted from (Hunger 2007)

| Class | Principal substrates | Method of application | Chemical types | Some examples |
|---|---|---|---|---|
| Acid | Nylon, wool, silk, paper, inks and leather | Usually from neutral to acidic dyebaths | Azo (including premetallized), anthraquinone, triphenylmethane, azine, xanthene, nitro and nitroso (Yagub et al. 2014) | Indian ink, congo red, nigrosoine |
| Azoic components and composition | Cotton, rayon, cellulose acetate any polyester | Fiber impregnated with coupling components and treated with solution of stabilized diazonium salt | Azo | Disperse orange 1, methyl orange |
| Basic | Paper, polyacrylonitrile, modified nylon, polyester and inks | Applied from acidic dyebaths | Cyanine, hemicyanine, diazahemicyanine, triarylmethane, azo, azine, xanthene, acridine, oxazine, and anthraquinone (Hunger 2007; Yagub et al. 2014; Mallakpour and Rashidimoghadam 2018; Siddiqui 2018) | Methylene blue, toluidine blue, thionine, and crystal violet |
| Direct | Cotton, rayon, paper, leather and nylon | Applied from neutral or slightly alkaline baths containing additional electrolyte | Azo, phthalocyanine, stilbene and oxazine (Yagub et al. 2014) | Direct light blue, direct light brilliant blue, direct copper blue 2R, direct diazo black BH |
| Disperse | Polyester, polyamide, acetate, acrylic and plastics | From solution dispersion or suspension in a mass | Stilbene, pyrazoles, coumarin, and naphthalimides (Aspland 1992) | Disperse orange 1, disperse red 9, disperse yellow 26 |

(continued)

**Table 6.2** (continued)

| Class | Principal substrates | Method of application | Chemical types | Some examples |
|---|---|---|---|---|
| Food, drug and cosmetic | The foods, the drugs and cosmetics | NA | Azo, anthraquinone, carotenoid and triarylmethane (Hunger 2007; Mallakpour and Rashidimoghadam 2018) | FD&C blue #1, D&C green #6 |
| Mordant | Wool, leather, and anodized aluminium | Applied in conjunction with Cr salts | Azo and anthraquinone (Hunger 2007; Mallakpour and Rashidimoghadam 2018) | Mordant brown 35 |
| Oxidation bases | Hair, fur, and cotton | Aromatic amines and phenol oxidized on the substrate | Aniline black and intermediate structures (Hunger 2007) | Basic yellow 57, basic red 76, basic blue 99 |
| Reactive | Cotton, wool, silk and nylon | Reactive site on dye reacts with functional group on fiber to bind dye covalently under influence of heat and pH (alkaline) | Azo, anthraquinone, phthalocyanine, formazan, oxazine, and basic (Hunger 2007; Mallakpour and Rashidimoghadam 2018) | Reactive blue 74, reactive brown 2, reactive yellow 4 |
| Solvent | Plastics, gasoline, varnishes, lacquers, strains, inks, fats, oils, waxes | Dissolves in the substrate | Azo, triphenylmethane, anthraquinone, and phthalocyanine (Hunger 2007) | Solvent red 24, solvent red 26, solvent red 164 |

**Table 6.3** Methods for dye removal (Siddiqui 2018)

| | |
|---|---|
| Physical methods | a. Precipitation/sedimentation<br>b. Coagulation<br>c. Filtration<br>d. Adsorption<br>e. Solvent extraction<br>f. Photocatalytic degradation |
| Chemical methods | a. Catalytic degradation<br>b. Chemical precipitation<br>c. Reduction<br>d. Oxidation<br>e. Ion exchange<br>f. Electrolysis<br>g. Fenton reaction |
| Biological methods | a. Fungal degradation<br>b. Algal treatment<br>c. Anaerobic digestion<br>d. Trickling filters<br>e. Activated sludge<br>f. Surface immobilization |

prepared by using the freeze drying method and then calcinated under the argon atmosphere. The aerogel was further calcinated in the air atmosphere at 450 °C for three different times (1, 2 and 3 h) of calcination. The $TiO_2$ aerogel was analyzed for the degradation of methyl orange under UV light irradiation. The result showed that the aerogel synthesized with a calcination time of 2 h has maximum photocatalytic activity.

Kim et al. (2013) used sol–gel synthesis to prepare the hydrophobic $TiO_2/SiO_2$ binary aerogel by using sodium silicate and titanium oxychloride as sodium and titanium precursors respectively. The aerogels were prepared with different silica to titanium ratios and were calcinated at various temperatures starting from 200 to 1000 °C. The photocatalytic activity of the aerogel was evaluated for the degradation of methylene blue (MB) under UV light radiation. As demonstrated in Fig. 6.5(a), the result showed that the binary composite with the weight ratio of 2(g of Si/g of Ti) exhibited the maximum activity. The photocatalytic activity of about 85% is maintained for three cycles as shown in Fig. 6.5(b).

Another study by Chang et al. (2014) reveals the preparation of $SiO_2/TiO_2$ composites under ambient pressure drying using the precursors such as tetraethoxysilane and tetrabutyl trinitrate. The prepared samples were heat-treated (calcinated) at 400–800 °C and are analyzed for the photocatalytic degradation of methylene blue dye. The result shows that the samples which were calcinated at 800 °C has better photocatalytic activity.

STAB (silica titania aerogel like balls) was synthesized by using sol–gel method followed by ball doping method (Xu et al. 2007). STAB samples were heat treated at various temperatures. The result shows that the STAB which was annealed at 600 °C has a maximum photocatalytic activity for the degradation of methylene blue dye.

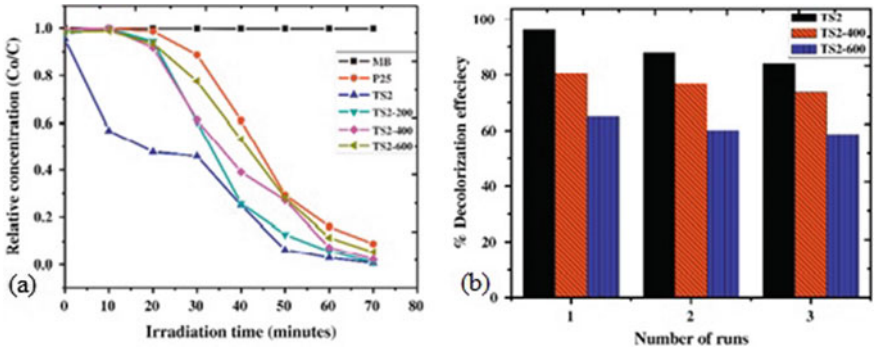


**Fig. 6.5** **a** Titania–silica aerogel photocatalyst degradation concentration versus time plot in decolorization of MB solution. **b** Evaluation of the reusability of TS2, TS2-400 and TS2-600 photocatalysts (Kim et al. 2013). Reproduced with permissions from reference (Kim et al. 2013)

Chemical liquid deposition of Ti onto nanoporous Si results in Si–Ti composite aerogels. The composite was synthesized by Zu et al. (2015) with different deposition cycles, i.e., by repeating the deposition procedure 5, 10 and 15 times. The prepared sample were calcinated at various temperatures in order to examine the heat effects. The Si–Ti composite aerogel which was synthesized by using 15 deposition cycles and calcinated at 600 °C shows the highest photodegradation efficiency toward methylene blue dye degradation.

Apart from inorganic aerogel, organic aerogel has also been synthesized using organic precursors like phenol–formaldehyde, melanin-formaldehyde, resorcinol–formaldehyde etc. The main properties of organic aerogels include less brittleness, greater stability, low weight and have great covalent bonds than the inorganic aerogels (Hasanpour and Hatami 2020).

The photocatalytic degradation of acridine orange under visible light irradiation was demonstrated by Jiang et al. (2019). The impact of various nitrogen precursors in nitrogen doped graphene aerogel on photocatalytic activity of acridine orange has been investigated. The maximum degradation was obtained for tetraethylenepentamine in nitrogen doped graphene aerogel. Polyaniline enhanced cellulose aerogel was synthesized using ionic liquid via a regeneration route by Zhou et al. (2014). The prepared aerogel was evaluated for the photodegradation activity toward the methylene blue (MB) dye using sunlight irradiation. The synthesized polyaniline enhanced cellulose aerogel showed outstanding photocatalytic activity with degradation efficiency of about 95% after 2 h.

To improve the dye degradation properties of the aerogel, two or more systems were combined to produce hybrid or composite material. In recent years the synthesis of inorganic–organic hybrid aerogels has been increased. The hybrid aerogels are majorly synthesized via sol–gel method. In these hybrid aerogels, carbon-based hybrid photocatalysts considering graphene and derivate were of main interest because of their large specific surface area, the broad spectrum of adsorption,

high adsorption capacity, high electrochemical stability, great electrical conductivity, outstanding mechanical strength and higher rates of adsorption–desorption (Hasanpour and Hatami 2020).

He et al. (2018) used a 2 step hydrothermal method to synthesize a novel 3D based graphene aerogel (GA)-carbon quantum dots (CQDs)/g-$C_3N_4$ nanosheet (CNN) composites aerogel with different mass ratios of Graphene Oxide to CNN (from 8 to 40%). The composites aerogel was evaluated for the photocatalytic degradation of the MO dye. The result showed that the GA/CQDs/CNN composite with a mass ratio of 24% has the highest MO dye removal performance of 91.1%. Factors that can contribute to the photocatalytic performance are the 3D porous structure, large specific surface area and the carbon quantum dots location on g-$C_3N_4$ nanosheet that considerably facilitate light collection and electron segregation.

Xiaolin et al. (2019) synthesized a composite aerogel by in situ deposition of Cu doped $Cu_2O$ on 3D graphene oxide (RGO)/cellulose (CE) aerogels. The prepared composite was compared with $Cu_2O$/CE aerogels for degradation efficiency of the photocatalyst toward methyl orange under irradiation of visible light. The effect of pH, the initial concentration of methyl orange solution and the amount of catalyst were studied and demonstrated in Fig. 6.6(a–c) respectively. The result shows that

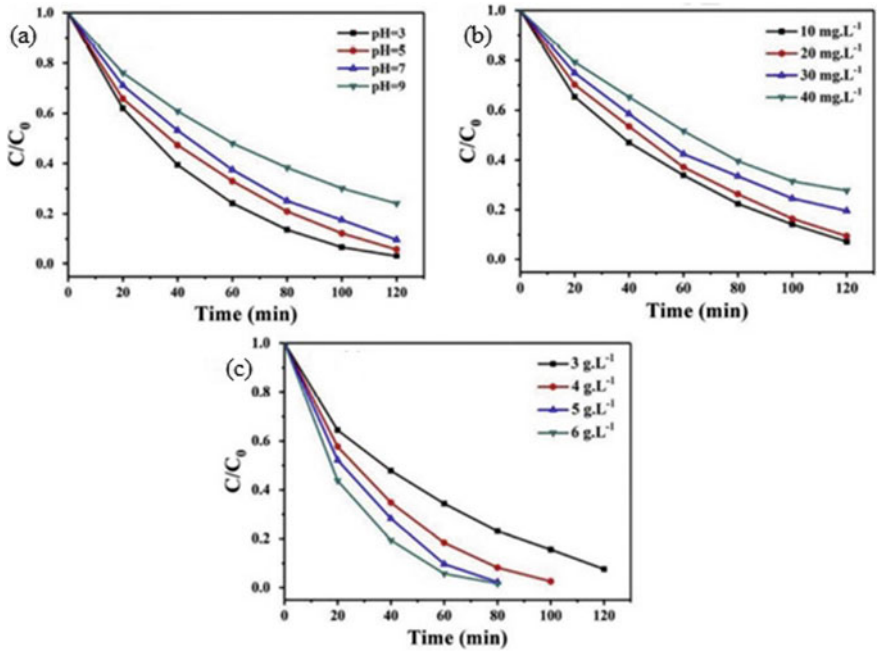


**Fig. 6.6** (**a**) Cu@$Cu_2O$/RGO/CE—effect of pH on MO photodegradation. (**b**) Cu@$Cu_2O$/RGO/CE—effect of initial concentrations of MO on photodegradation. (**c**) Cu@$Cu_2O$/RGO/CE—effect of catalyst loading on MO photodegradation. Reproduced with permissions from reference (Xiaolin et al. 2019)

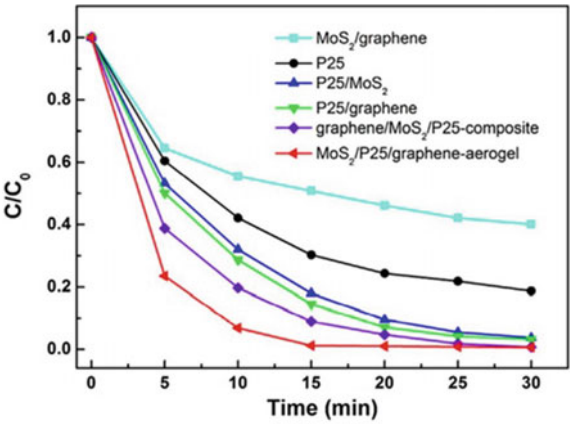


**Fig. 6.7** Photo-degradation of methyl orange by $MoS_2/TiO_2(P2)_5$/graphene-aerogel(GA), graphene/$TiO_2$(P25)/$MoS_2$-composite, $TiO_2$(P25)/graphene, $MoS_2/TiO_2$(P25), $MoS_2$/graphene, and $TiO_2$(P25) with reaction time of 30 min under UV irradiation (Han et al. 2014). Reproduced with permissions from reference (Han et al. 2014)

the hybrid catalyst of Cu@$Cu_2O$/RGO/CE has higher photocatalytic activity when compared to $Cu_2O$/CE aerogels.

Fan et al. (2015) described the synthesis of novel photocatalyst material made of AgX (where X = Cl, Br) doped on the 3D graphene aerogel (GA) surface. The prepared sample was evaluated for the photodegradation efficiency toward methyl orange (MO) under visible light irradiation. The result obtained shows that the MO can almost completely be removed by AgBr/GA while the pure AgBr can only remove 65% of the MO. Similarly, the photodegradation efficiency of AgCl/GA was high when compared with bare AgCl.

Han et al. (2014) synthesized the 3D molybdenum disulfide ($MoS_2$)/$TiO_2$(P25)/graphene aerogel (GA) by hydrothermal method. The synthesized composite was compared with $TiO_2$/GA, $MoS_2$/GA, $MoS_2/TiO_2$ by evaluating the degradation efficiency against the removal of methyl orange under ultraviolet light radiation. As shown in Fig. 6.7, the degradation efficiency of almost 100% was achieved by $MoS_2/TiO_2$(P25)/graphene aerogel (GA) within 15 min.

Wei et al. (2019a) created a new 3D based cadmium sulfide (CdS)/graphene aerogel (GA) by a one-pot hydrothermal method. The CdS-GA's photocatalytic activity was analyzed for the elimination of organic pollutants in water. The removal of organic pollutant efficiency was high for the CdS/GA composite hybrid aerogel in comparison with pure CdS and GA. In the case of methyl orange removal, the CdS/GA hybrid shows 98.8% efficiency within 60 min, according to their finding shown in Fig. 6.8.

Bin et al. (2015) synthesized the novel 3D graphene-Cobalt(II,III) oxide ($Co_3O_4$) composite by using freeze-drying and calcination techniques. Synthesized graphene oxide by hummer's method was added to the Cobalt nitrate solution and then freeze-dried followed by calcination in order to produce 3D GA/$Co_3O_4$ hybrid aerogels. The hybrid aerogels were prepared by varying the GO to Cobalt nitrate weight ratios (0, 1, 2, 3%). The hybrid aerogels were analyzed for the photocatalytic activity of methyl orange under a xenon arc lamp as the light source. The highest degradation

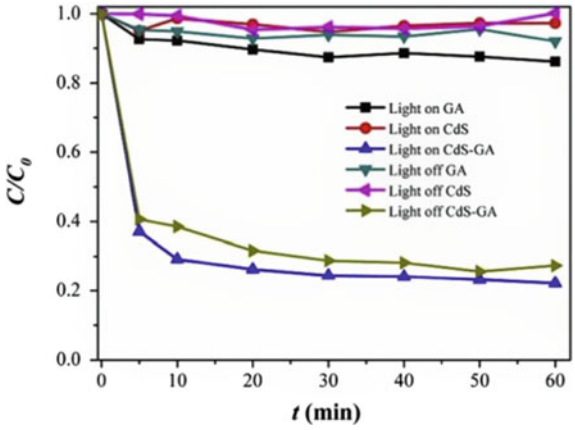


**Fig. 6.8** The degradation performance of CdS, GA and the CdS-GA hybrids for methyl orange dye in water (Wei et al. 2019a). Reproduced with permissions from reference (Wei et al. 2019a)

efficiency of 95.3% was shown by3D GA/$Co_3O_4$ hybrid aerogels synthesized with a 2% weight ratio of GO to Cobalt nitrate. They also demonstrated that magnetic decantation could efficiently separate samples from the reaction media.

Yang et al. (2017) synthesized a novel 3D-3D Bismuth tungstate ($Bi_2WO_6$)-Graphene hydrogel (GH) by using the hydrothermal and freeze-drying method as demonstrated in Fig. 6.9(a). The hydrogels were prepared by changing the molar quantities of precursors used for making $Bi_2WO_6$ and keeping the graphene oxide solution volume constant. The $Bi_2WO_6$/GH samples were analyzed for photocatalytic activity against the degradation of methylene blue under the region of UV and visible light. The hydrogel shows refer to Fig. 6.9(b) better photocatalytic activity than pure Bismuth tungstate because the presence of graphene in the composite improves the photocatalytic efficiency.

Melone et al. (2013) prepared hybrid aerogels by mixing cellulose nanofibers (CNF) with either $TiO_2$(T) sol or $TiO_2/SiO_2$(TS) sol. The prepared aerogels were

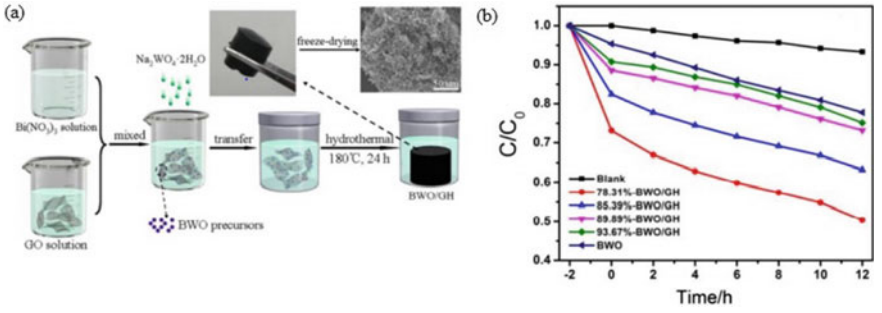


**Fig. 6.9** (**a**) Schematic demonstration of the preparation process of 3D-$Bi_2WO_6$/GH composite. (**b**) The removal of Methylene Blue by $Bi_2WO_6$ and $Bi_2WO_6$/GH composites under visible light source irradiation (Yang et al. 2017). Reproduced with permissions from reference (Yang et al. 2017)

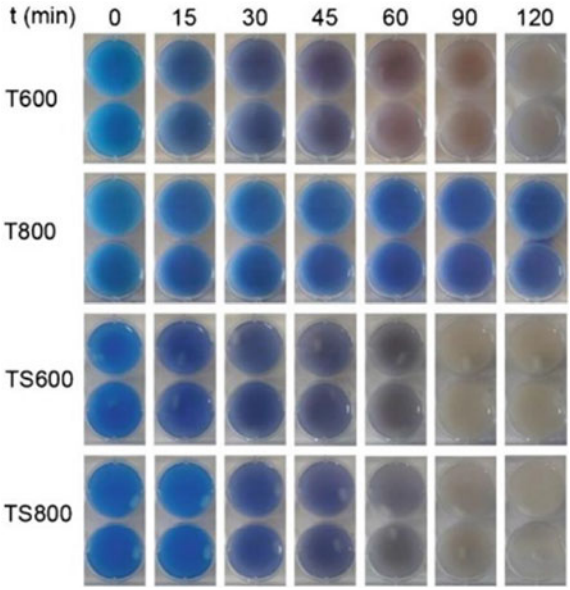


**Fig. 6.10** MB degradation analysis under ultra violet irradiation on TX and TSX aerogels where X is the calcination temperature (Melone et al. 2013). Reproduced with permissions from reference (Melone et al. 2013)

calcinated at various temperatures. The absorption experiment with methylene blue (MB) and Rhodamine B (RhB) dyes was conducted in order to check degradation effects. In the case of MB degradation, the CNF-$TiO_2$ aerogel which is calcinated 600 °C (T600) shows higher efficiency than the sample calcinated at 800 °C (T800) and the result are shown in Fig. 6.10. The CNF-$TiO_2$/$SiO_2$ shows better efficiency when compared to CNF-$TiO_2$ at both calcination temperatures for the degradation of MB. In the case of RhB degradation, the degradation by CNF-$TiO_2$ was negligible at both the calcination temperatures and the CNF-$TiO_2$/$SiO_2$ aerogel shows that by increasing the annealing temperature, the efficiency increases.

Wei et al. (2019b) effectively synthesized unique 2D based nanorods of bismuth phosphate (BP)/3D biomass-based carbonaceous aerogels (BCA) composite by hydrothermal process. The aerogels were prepared at different BP/BCA weight percentages of 5, 10, 20, 30 and 40. The composite aerogels were evaluated for the degradation of methylene blue dye under UV light irradiation for about 180 min. The BP/BCA composite aerogel with 20 weight percent shows the highest photocatalytic activity of about 71.9%, followed by 10 weight percent composite which shows about 52.8% activity.

Zhang et al. (2019) fabricated a Graphene Oxide (GO)-Titanium dioxide ($TiO_2$)-Carbon Quantum Dots (CQD) foam by a simple and low-cost solvothermal method. The prepared form was analyzed in order to check the degradation efficiency of the methyl orange (MO), methylene blue (MB) and Rhodamine B (RhB) dyes under the light source of a xenon lamp. The result shows that GO-$TiO_2$-CQD foam has high degradation efficiency of 92.48% toward MO, 95.5% toward MB (shown in Fig. 6.11) and 92.84% toward are RhB when compared to Graphene Oxide foam,

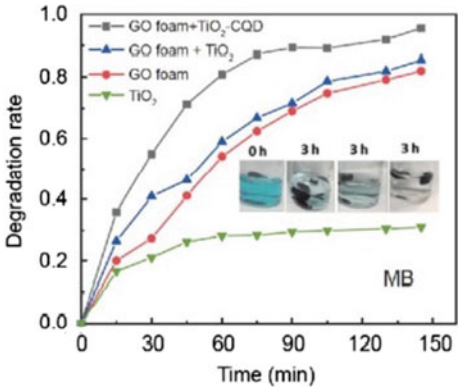


**Fig. 6.11** Photocatalytic degradation kinetics of MB (Zhang et al. 2019). Reproduced with permissions from reference (Zhang et al. 2019)

Graphene Oxide-$TiO_2$ foam and $TiO_2$ powder. The composite foam maintains a high degradation rate and stability even after many cycles of usage.

#### 6.2.2.1 Photocatalysis Using Aerogel Materials

Photocatalysis is a process that can be used to resolve related environmental issues originated by organic pollutants, posing a big threat to human life and ecosystem (Qi and Yu 2020). Photocatalysis carried out with powder samples normally have the attitude to cluster and for recycling the intricate procedure, it will limit the practical applications.

The 3D porous solid network aerogels are the ones that have very low density, huge specific surface area and high porosity. It consists of nano-scale characteristics with an overall monolith size of various cm. Therefore, aerogels are considered as a bridge connecting the nano and the macro within that building block; it not only holds the pristine properties, but it does form a fresh function through the three-dimensional action of the building block (Aegerter et al. 2011). Aerogel is very special for photocatalytic applications. After the improvement in synthesis technologies, the forms of aerogel photocatalysts have increased from the conventional oxide and the chalcogenide aerogels to the recent composite aerogel. And also, their application extended from the primary physical adsorption to the current photochemical reaction that includes the environmental correction and clean energy manufacture (Serhan et al. 2019).

In order to understand the photocatalytic activity of aerogel materials, let us consider the example of graphene aerogel and CdS aerogel. Table 6.4 shows the photocatalytic degradation of the RhB organic dyes in the water with different graphene aerogel photocatalysts (Long et al. 2020).

Graphene aerogel under photocatalysis can also be used for the separation of uranium from the water below visible light and in the air atmosphere. For this process, a novel graphene aerogel is prepared, GA-200. Uranium has photochemical property, due to which it plays a major role to create $H_2O_2$ with $O_2$ in the air, and it forms

**Table 6.4** Photocatalytic degradation of the RhB organic dyes in the water with the different graphene aerogel supported photocatalysts (Long et al. 2020). Reproduced with permissions from reference (Long et al. 2020)

| Photocatalyst (mg) | Pollutant (mg/L) | Light (W) | Degradation (%) | Time (min) | Cycle | Cyclic effect | Refs. |
|---|---|---|---|---|---|---|---|
| $Ag_2O$/ALG-rGO (30) | RhB (Vacher et al. 1988) | 500 W Xe lamp | 96 | 150 | 5 | 89% | Ma et al. (2018) |
| $Bi_2WO_6$/ GA (20) | RhB (Gesser and Goswami 1989) | 300 W Xe lamp | 99.6 | 45 | ND | ND | Xu et al. (2016b) |
| BiOBr/RGO aerogel | RhB | 300 W Xe lamp | Over 68 | ND | 5 | 68% | Liu et al. (2015) |
| $CeO_2$/RGO | RhB | 150 W Xe lamp | 85 | 120 | 3 | No significant changes | Choi et al. (2016) |
| BiOBr/RGO | RhB | 300 W Xe lamp | 50 | 60 | ND | ND | Yu et al. (2017a) |
| g-$C_3N_4$-$TiO_2$-GA (5) | RhB (Peng et al. 2021) | 500 W Xe lamp | 98.40 | 60 | 4 | 75.60% | Zhang et al. (2018a) |
| $Fe_2O_3$-$TiO_2$-GA | RhB (Peng et al. 2021) | 500 W Xe lamp | 97.70 | 60 | 4 | 81.80% | Zhang et al. (2018b) |
| $W_{18}O_{49}$-RGO | RhB | 500 W Xe lamp | 100 | 25 | 30 | No significant changes | Li et al. (2014) |
| $TiO_2$-GA (5) | RhB (Peng et al. 2021) | 300 W Xe lamp | 98.7 | 180 | 5 | 70% | Zhang et al. (2016) |
| 3D Ag/Ag$^{@}$$Ag_3PO_4$/GA (7.5) | RhB (Torikai et al. 1994) | 400 W Xe lamp | 100.0% | 15 | 6 | No significant changes | Chen et al. (2018) |
| 3D g-$C_3N_4$/BiOBr/RGO | RhB | 300 W Xe lamp | 66 | 60 | 3 | No significant changes | Yu et al. (2017b) |

*RGO* reduced graphene oxide, *GA* grapheme aerogel, *RhB* rhodamine B

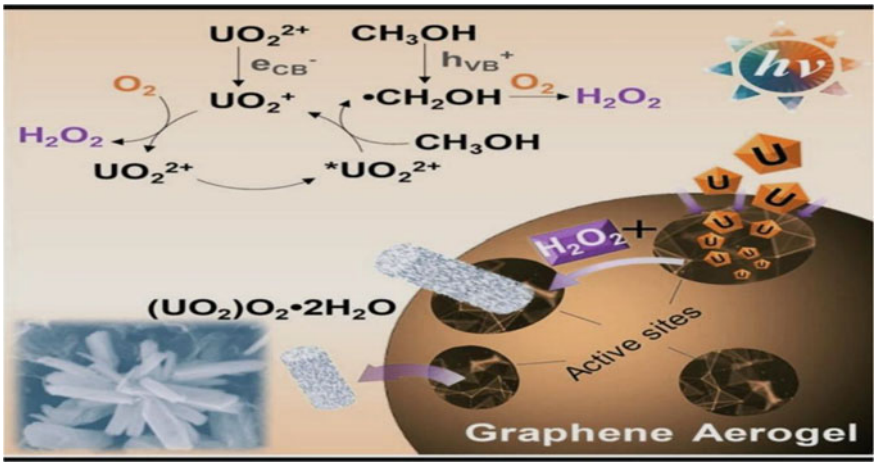


**Fig. 6.12** Schematic representation of uranium removal using graphene aerogel (Wang et al. 2020). Reproduced with permissions from reference (Wang et al. 2020)

$(UO_2)O_2.2H_2O$. The products that are neutral can empty from the surface of the GA-200, and thus, it regenerates the active sites in situ. This results on the separation capacity of 1050 mg/g (Wang et al. 2020) (Fig. 6.12).

CdS aerogels synthesized by the normal sol–gel assembly of the individual nanocrystals into a porous channel, which is accompanied by a supercritical drying method, can give high surface area for photocatalytic degradation. The evaluation to understand the quality of CdS aerogel for the dye degradation of organic dyes was done using methylene blue and methyl orange as the test molecule. After analysis, it was found that the CdS aerogel material showed impressive photocatalytic activity for degradation of dyes when compared with the typical ligand capped CdS nanocrystals. The catalytic efficiency of the CdS aerogel can be increased by decreasing the length of the chain and extending the surface organics that lead to more and higher hydrophilic reachable surface area (Korala et al. 2017).

## 6.3 Conclusion

Aerogels, due to their high absorption rate and properties, can be explored for a wide range of applications, and it has been proven that they can be used as a promising solution for dye removal. Dyes are used in different industries like Textile, Food, Paper, Cosmetic, Leather, Fur with the textile industry as a major consumer. Researchers believe photocatalysts with the 3D porous network structures (aerogels) to be the most likely materials for water purification in recent periods. Characteristic features like exceptionally high porosity, huge specific surface area, very low

density, and ease of detachment from aqueous solution etc. make these materials suitable for dye removal. Photocatalytic characteristics of the aerogels can be changed through combining them with diverse materials such as organic, inorganic and hybrid. Because of the large specific surface area, the high sorption capacity, great electrical conductivity, advanced electrochemical stability, superior mechanical strength, and advanced adsorption–desorption rates, new studies have displayed that the carbon-based hybrid aerogels considering graphene and derivatives as photocatalysts can effectively remove pollutants, especially the organic dyes from wastewater.

## References

Aegerter MA, Leventis N, Koebel MM (2011) Aerogels handbook. Springer

Aspland JR (1992) A series on dyeing. Chapter 8: disperse dyes and their application to polyester. Text Chem Color 24:8–13

Bin Z, Hui L (2015) Three-dimensional porous graphene-$Co_3O_4$ nanocomposites for high performance photocatalysts. Appl Surf Sci 357:439–444

Chen F et al (2018) 3D graphene aerogels-supported Ag and Ag@$Ag_3PO_4$ heterostructure for the efficient adsorption-photocatalysis capture of different dye pollutants in water. Mater Res Bull 105:334–341

Cheng S, Liu X, Yun S, Luo H, Gao Y (2014) $SiO_2$/$TiO_2$ composite aerogels: preparation via ambient pressure drying and photocatalytic performance. Ceram Int 40:13781–13786

Choi J, Reddy DA, Islam MJ, Ma R, Kim TK (2016) Self-assembly of $CeO_2$ nanostructures/reduced graphene oxide composite aerogels for efficient photocatalytic degradation of organic pollutants in water. J Alloys Compd 688:527–536

Du A, Zhou B, Zhang Z, Shen J (2013) A special material or a new state of matter: a review and reconsideration of the aerogel. Materials (Basel) 6:941–968

Fan Y et al (2015) Convenient recycling of 3D AgX/graphene aerogels (X = Br, Cl) for efficient photocatalytic degradation of water pollutants. Adv Mater 27:3767–3773

Fricke J (1988) Aerogels—highly tenuous solids with fascinating properties. J Non Cryst Solids 100:169–173

Fricke J, Emmerling A (1998) Aerogels—recent progress in production techniques and novel applications. J Sol-Gel Sci Technol 13:299–303

Fricke J, Emmerling A (1992) Aerogels—preparation, properties, applications:37–87. https://doi.org/10.1007/bfb0036965

Gesser HD, Goswami PC (1989) Aerogels and related porous materials. Chem Rev 89:765–788

Gurav JL, Jung IK, Park HH, Kang ES, Nadargi DY (2010) Silica aerogel: synthesis and applications. J Nanomater 2010

Hamaker HC (1937) A general theory of lyophobic colloids. II. Recl des Trav Chim des Pays-Bas 56:3–25

Han W et al (2014) Enhanced photocatalytic activities of three-dimensional graphene-based aerogel embedding $TiO_2$ nanoparticles and loading $MoS_2$ nanosheets as co-catalyst. Int J Hydrogen Energy 39:19502–19512

Hasanpour M, Hatami M (2020) Photocatalytic performance of aerogels for organic dyes removal from wastewaters: review study. J Mol Liq 309:113094

He H, Huang L, Zhong Z, Tan S (2018) Constructing three-dimensional porous graphene-carbon quantum dots/g-$C_3N_4$ nanosheet aerogel metal-free photocatalyst with enhanced photocatalytic activity. Appl Surf Sci 441:285–294

Hunger K (2007) Industrial dyes: chemistry, properties, applications. Wiley

Jiang Y, Chowdhury S, Balasubramanian R (2019) New insights into the role of nitrogen-bonding configurations in enhancing the photocatalytic activity of nitrogen-doped graphene aerogels. J Colloid Interface Sci 534:574–585

Kim YN et al (2013) Sol–gel synthesis of sodium silicate and titanium oxychloride based $TiO_2$–$SiO_2$ aerogels and their photocatalytic property under UV irradiation. Chem Eng J 231:502–511

Korala L et al (2017) CdS aerogels as efficient photocatalysts for degradation of organic dyes under visible light irradiation. Inorg Chem Front 4:1451–1457

Li K, Zhang X, Qin Y, Li Y (2021) Construction of the cellulose nanofibers (Cnfs) aerogel loading tio2 nps and its application in disposal of organic pollutants. Polymers (Basel) 13

Li X et al (2014) Tungsten oxide nanowire-reduced graphene oxide aerogel for high-efficiency visible light photocatalysis. Carbon 78:38–48

Liu W, Cai J, Li Z (2015) Self-assembly of semiconductor nanoparticles/reduced graphene oxide (RGO) composite aerogels for enhanced photocatalytic performance and facile recycling in aqueous photocatalysis. ACS Sustain Chem Eng 3:277–282

Liu Z et al (2021) Synthesis of mesoporous carbon nitride by molten salt-assisted silica aerogel for rhodamine B adsorption and photocatalytic degradation. J Mater Sci 56:11248–11265

Long S et al (2020) 3D graphene aerogel based photocatalysts: synthesized, properties, and applications. In: Colloids and surfaces A: physicochemical and engineering aspects, vol 594. Elsevier B.V.

Ma Y, Wang J, Xu S, Feng S, Wang J (2018) $Ag_2O$/sodium alginate-reduced graphene oxide aerogel beads for efficient visible light driven photocatalysis. Appl Surf Sci 430:155–164

Mallakpour S, Rashidimoghadam S (2018) Carbon nanotubes for dyes removal. In: Composite nanoadsorbents. Elsevier Inc. https://doi.org/10.1016/B978-0-12-814132-8.00010-1

Maouche C et al (2020) A 3D nitrogen-doped graphene aerogel for enhanced visible-light photocatalytic pollutant degradation and hydrogen evolution. RSC Adv 10:12423–12431

Matsuda H, Kobayashi N, Kobayashi T, Miyazawa K, Kuwabara M (2000) Room-temperature synthesis of crystalline barium titanate thin films by high-concentration sol-gel method. J Non Cryst Solids 271:162–166

Melone L et al (2013) Ceramic aerogels from TEMPO-oxidized cellulose nanofibre templates: synthesis, characterization, and photocatalytic properties. J Photochem Photobiol A Chem 261:53–60

Nita LE, Ghilan A, Rusu AG, Neamtu I, Chiriac AP (2020) New trends in bio-based aerogels. Pharmaceutics 12

Peng YH, Kashale AA, Lai Y, Hsu FC, Chen IWP (2021) Exfoliation of 2D materials by saponin in water: aerogel adsorption/photodegradation organic dye. Chemosphere 274:129795

Pierre AC, Pajonk GM (2002) Chemistry of aerogels and their applications. Chem Rev 102:4243–4265

Qi K, Yu J (2020) Modification of ZnO-based photocatalysts for enhanced photocatalytic activity. Interface Sci Technol 31:265–284

Said B, El Harfi S, El Harfi A (2017) Classifications, properties and applications of textile dyes: a review. Appl J Environ Eng Sci 3:311–320

Schaedler TA et al (2011) Ultralight metallic microlattices. Science 334:962–965

Schaefer DW, Keefer KD (1986) Structure of random porous materials: silica aerogel. Phys Rev Lett 56:2199–2202

Serhan M et al (2019) Total iron measurement in human serum with a smartphone. In: AIChE annual meeting of conference on proceeding, 2019 Nov

Siddiqui SI et al (2018) Decolorization of textile wastewater using composite materials. Nanomater Wet Process Text:187–218. https://doi.org/10.1002/9781119459804.ch6

Torikai D et al (1994) Comparison of high-purity $H_2/O_2$ and LPG/$O_2$ flame-fused silica glasses from sol-gel silica powder. J Non Cryst Solids 179:328–334

Vacher R, Woignier T, Pelous J, Courtens E (1988) Structure and self-similarity of silica aerogels. Phys Rev B 37:6500–6503

Wagh PB, Begag R, Pajonk GM, Venkateswara Rao A, Haranath D (1999) Comparison of some physical properties of silica aerogel monoliths synthesized by different precursors. Mater Chem Phys 57:214–218

Wang Z et al (2020) Graphene aerogel for photocatalysis-assist uranium elimination under visible light and air atmosphere. Chem Eng J 402:126256

Wei XN et al (2019a) One-pot self-assembly of 3D CdS-graphene aerogels with superior adsorption capacity and photocatalytic activity for water purification. Powder Technol 345:213–222

Wei W et al (2019b) $BiPO_4$ nanorods anchored in biomass-based carbonaceous aerogel skeleton: a 2D–3D heterojunction composite as an energy-efficient photocatalyst. J Supercrit Fluids 147:33–41

Wen J, Liu H, Zheng Y, Wu Y, Gao J (2020) A novel of PTA/ZIF-8@cellulose aerogel composite materials for efficient photocatalytic degradation of organic dyes in water. Zeitschrift Fur Anorg Und Allg Chemie 646:444–450

Wu Y et al (2020) Zeolitic imidazolate framework-67@cellulose aerogel for rapid and efficient degradation of organic pollutants. J Solid State Chem 291:121621

Xiaolin D et al (2019) High photocatalytic activity of Cu@$Cu_2O$/RGO/cellulose hybrid aerogels as reusable catalysts with enhanced mass and electron transfer. React Funct Polym 138:79–87

Xu Z et al (2007) Preparation and characterization of silica-titania aerogel-like balls by ambient pressure drying. J Sol-Gel Sci Technol 41:203–207

Xu H, Zhu P, Wang L, Jiang Z, Zhao S (2016a) Structural characteristics and photocatalytic activity of ambient pressure dried $SiO_2$/$TiO_2$ aerogel composites by one-step solvent exchange/surface modification. J Wuhan Univ Technol Mater Sci Ed 31:80–86

Xu X, Ming F, Hong J, Xie Y, Wang Z (2016b) Three-dimensional porous aerogel constructed by $Bi_2WO_6$ nanosheets and graphene with excellent visible-light photocatalytic performance. Mater Lett 179:52–56

Yagub MT, Sen TK, Afroze S, Ang HM (2014) Dye and its removal from aqueous solution by adsorption: a review. Adv Colloid Interface Sci 209:172–184

Yang J, Chen D, Zhu Y, Zhang Y, Zhu Y (2017) 3D–3D porous $Bi_2WO_6$/graphene hydrogel composite with excellent synergistic effect of adsorption-enrichment and photocatalytic degradation. Appl Catal B Environ 205:228–237

Yu X, Shi J, Feng L, Li C, Wang L (2017a) A three-dimensional BiOBr/RGO heterostructural aerogel with enhanced and selective photocatalytic properties under visible light. Appl Surf Sci 396:1775–1782

Yu X et al (2017b) Ternary-component reduced graphene oxide aerogel constructed by g-$C_3N_4$/BiOBr heterojunction and graphene oxide with enhanced photocatalytic performance. J Alloys Compd 729:162–170

Zhang JJ et al (2016) Synergetic adsorption and photocatalytic degradation of pollutants over 3D $TiO_2$-graphene aerogel composites synthesized: via a facile one-pot route. Photochem Photobiol Sci 15:1012–1019

Zhang JJ et al (2018a) High-efficiency removal of rhodamine B dye in water using g-$C_3N_4$ and $TiO_2$ co-hybridized 3D graphene aerogel composites. Sep Purif Technol 194:96–103

Zhang JJ et al (2018b) Three-dimensional $Fe_2O3$–$TiO_2$–graphene aerogel nanocomposites with enhanced adsorption and visible light-driven photocatalytic performance in the removal of RhB dyes. J Ind Eng Chem 61:407–415

Zhang X, Wei W, Zhang S, Wen B, Su Z (2019) Advanced 3D nanohybrid foam based on graphene oxide: facile fabrication strategy, interfacial synergetic mechanism, and excellent photocatalytic performance. Sci China Mater 62:1888–1897

Zhang B et al (2018) Bacterial cellulose derived monolithic titania aerogel consisting of 3D reticulate titania nanofibers. Cellulose 25:7189–7196

Zhou Z, Zhang X, Lu C, Lan L, Yuan G (2014) Polyaniline-decorated cellulose aerogel nanocomposite with strong interfacial adhesion and enhanced photocatalytic activity. RSC Adv 4:8966–8972

Zu G et al (2015) Silica-titania composite aerogel photocatalysts by chemical liquid deposition of titania onto nanoporous silica scaffolds. ACS Appl Mater Interfaces 7:5400–5409